CHAPTER 4

SALOPHEN-BASED TETRADENTATE [N_2O_2]-DONOR SCHIFF BASE COMPLEXES OF OXOVANADIUM(IV), NICKEL(II) AND COPPER(II)

CHAPTER 4

SALOPHEN-BASED TETRADENTATE $[N_2O_2]$-DONOR SCHIFF BASE COMPLEXES OF OXOVANADIUM(IV), NICKEL(II) AND COPPER(II)

4.1 Introduction:

Schiff base with 'salophen' type fragment as core unit in metal containing liquid crystals have drawn significant attention owing to the possibility of combining optical, electronic and magnetic characteristics, supramolecular properties with those of anisotropic fluidity.[1-7] Transition metal complexes with salen-type ligands have been extensively studied mainly due to their ability to catalyze an extremely broad range of chemical transformations including the asymmetric ring-opening of epoxides, aziridination, cyclopropanation, epoxidation of olefins and formation of cyclic and linear polycarbonates.[8-11] Choice of metal ion, nature and position of the substituents on side aromatic ring as well as spacers are known to greatly tune the mesogenic as well as photophysical behaviour. For some compounds even a minor changes within the spacer can lead to major differences in molecular organization and in turn liquidcrystalline behaviour.[12-19] The technologies based on physical properties such as light emission or charge transport ability and related materials are currently receiving significant attention owing to their potential applications such as solar cells, active components for image and data treatment storage, organic light emitting diodes (OLEDs), sensors, enhanced contrast displays, novel ferroelectric/piezoelectric and non-linear optical (NLO) materials.[20-26] Metallomesogens (metal containing liquid crystals) are ideal candidates for tuning smart multifunctional properties. Studies on light-emitting mesogens were mainly focused on organic compounds, while luminescent metallomesogens caught the fancy of researchers rather recently.[1-5, 27]

Compounds that form columnar discotic liquid crystalline mesophases with axially linked discs are of particular interest as potential one-dimensional photoconductors, semiconductors, organic light emitting diodes and photovoltaic cells.[28-33]

Metal-salen complexes with 5-substituted alkoxy or alkyl chains exhibiting smectic mesomorphism are well documented.[34-37] Metallomesogen based on 4-substituted salen-type framework Schiff base ligands has been sparsely investigated.[4-6, 12]

Set in this backdrop we embarked on the synthesis of Ni(II), VO(IV) and Cu(II), complexes of 'salophen' type Schiff base ligand with or without substituent on aromatic spacer group and explore their mesomorphic and photoluminescence behaviour. The ligands are non-mesogenic and devoid of any luminescence.

4.2 Experimental:

4.2.1 Synthesis of mononuclear nickel-salophen complex:

The synthesis of Schiff base ligands (16-opd/16-mpd) were carried out by condensation of 4-alkoxysubstituted aldehyde with unsubstituted/methyl-substituted 1, 2-phenylene diamine as per procedure reported earlier.[14,15] A new series of mononuclear nickel(II) complexes of the type (Ni-16opd/Ni-16mpd) have been synthesised and are presented in **Scheme1**.

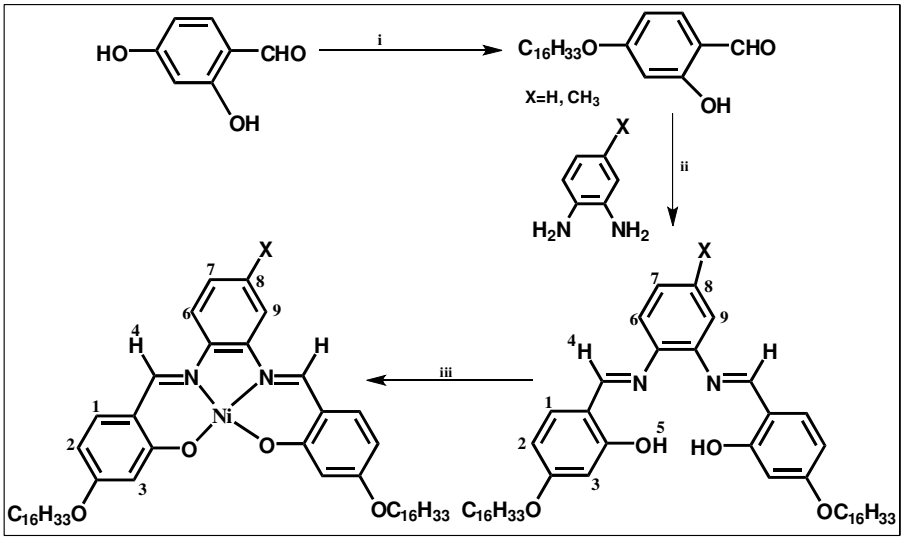

Scheme1. i.$C_{16}H_{33}Br$, $KHCO_3$, KI, dry acetone, Δ, 40h, and ii. glacial AcOH, absolute EtOH Δ, 4h iii.$Ni(OAc)_2.4H_2O$, MeOH, Stir, 2h

Synthesis of nickel (II) complexes:

The ligand 16-opd (0.79g, 1mmol) or 16-mpd (0.81g, 1mmol) was dissolved in minimum volume of absolute ethanol. To this, an equimolar amount of nickel acetate $Ni(OAc)_2.4H_2O$(0.24g, 1mmol) in methanol was then added slowly and stirred for 2h

at room temperature. A red solid formed immediately was filtered, washed with diethyl ether and recrystallized from chloroform-ethanol (1:1).

Ni- 16opd:

Yield = 0.60g (75%). FAB Mass (m/e, fragment): m/z: calc. 852.5; found: 853.5[M+H^+]; Anal. Calc. for $C_{52}H_{78}N_2O_4Ni$: C, 73.1; H, 9.2; N 3.2. Found: C, 73.1; H, 9.2; N, 3.1%. ^{1}H NMR (400 MHz, $CDCl_3$): δ = 8.22 (s, 1H, H^4), 7.69 (d, J = 8.5Hz, H^9), 7.17 (d, 2H, H^6), 7.10 (t, J = 8.4 Hz, 2H, H^1), 7.16 (dd, J = 2.3 Hz, J = 9.1, 2H, H^8), 6.61 (d, J = 2.4 Hz, 2H, H^3), 6.49 (dd, J = 2.4 Hz, J = 8.2 Hz, 2H, H^2), 3.95 (t, J = 6.8 Hz, 2H, -OCH_2), 0.91 (t, J=6.8Hz, 6H, CH_3), 0.87 (m, -CH_2 of methylene proton in side chain); IR (ν_{max}, cm^{-1}, KBr): 2922 ($\nu_{as(C-H),}CH_3$), 2870 ($\nu_{s(C-H),}CH_3$), 1611 ($\nu_{C=N}$), 534(ν_{Ni-N}), 459(ν_{Ni-O}).

Ni- 16mpd:

Yield = 0.22g, 76%. FAB Mass (m/e, fragment): m/z: calc. 866.5; found: 867.5[M+H^+]; Anal. Calc. for $C_{53}H_{80}N_2O_4Ni$: C, 73.3; H, 9.2; N 3.2. Found: C, 73.4; H, 9.3; N, 3.1%. ^{1}H NMR (400 MHz, $CDCl_3$): δ = 8.19 (s, 1H, H^4), 7.72 (d, J = 8.5Hz, H^9), 7.21 (d, 2H, H^6), 7.11 (t, J = 8.4 Hz, 2H, H^1), 7.16 (dd, J = 2.33 Hz, J = 9.1, 2H, H^8), 6.61 (d, J = 2.4 Hz, 2H, H^3), 6.49 (dd, J = 2.44 Hz, J = 8.28 Hz, 2H, H^2), 3.92 (t, J = 6.8 Hz, 2H, -OCH_2), 0.91 (t, J=6.8Hz, 6H, CH_3), 0.87 (m, -CH_2 of methylene proton in side chain); IR (ν_{max}, cm^{-1}, KBr): 2922 ($\nu_{as(C-H),}CH_3$), 2870 ($\nu_{s(C-H),}CH_3$), 1613 ($\nu_{C=N}$), 532(ν_{Ni-N}), 461(ν_{Ni-O}).

4.2.1.1 Results and discussion:

Synthesis and structural assessment:

The synthetic procedure of the ligands are describrd in our earlier report.[14,15] The compounds (16-opd/16-mpd and Ni-16opd/Ni-16mpd) could be achieved through a facile and straightforward procedure.[14,15] The synthetic strategy for the ligands [(L = N, N′-bis (4-(4′-n-hexadecyloxy)-salicylidene) 1,2-phenylenediamine/4-Me-1, 2-phenylenediamine), hereafter abbreviated as 16-opd/16-mpd] and the Ni(II) complexes (Ni-16opd/Ni-16mpd) are presented in **Scheme 1**.

The complexes (Ni-16opd/Ni-16mpd) were prepared by the reaction of appropriate ligand with nickel acetate (1:1 molar ratio) in ethanol/methanol and recrystallised from methanol/CH_2Cl_2; the complexes were isolated as red coloured solids in good

yields. The compounds were characterized by ^{1}H NMR, FT-IR, UV-Vis spectroscopy and elemental analysis. From the IR Study, it was found that the shift of ν_{CN} vibrational stretching frequency at ca.1625cm^{-1} to lower wave number ($\Delta\nu$ ~30cm^{-1}) and absence of ν_{OH} mode upon chelation, clearly suggested the coordination of azomethine-N and phenolate-O to the metal. Appearance of additional bands at ~450-480 and ~527-549cm^{-1} in the spectra of the complexes assigned to Ni–O and Ni–N stretching vibrations that are not observed in the spectra of the ligands furnished evidence for [N,O] binding mode of the ligand. The $\nu_{C=N}$ stretching frequency is rather independent of the length of alkoxy side chain in both ligands and their complexes. The FAB-mass spectra of the compounds matched well with their formula weights. Solution electrical conductivity of complexes recorded in CH_2Cl_2 (10^{-3}M) was found to be $< 10\ \Omega^{-1}cm^{-1}mol^{-1}$, much lower than is expected for a 1:1 electrolyte, thus confirming the non-electrolytic nature of the complex. ^{1}H NMR spectra of the ligands showed two characteristic signals at δ = 13.4-13.8ppm corresponding to the OH proton and at δ = 8.5 ppm due to the imine proton. Moreover upon complexation, lack of proton signal corresponding to the OH group of the free ligands and the upfield shift of the imine proton further attested the coordination of azomethine-N.

Photophysical properties:

The electronic spectra of the free ligands exhibited three bands (**Fig.1**) in the region of ~288-366 nm assigned to π-π* transitions which involves molecular orbitals essentially localized on the C=N group and the benzene ring. The complexes exhibited two intense red shifted bands (**Fig.2**) at ~312-325nm and ~383-401nm resulting from the metal-perturbed ligand-centred transitions which have the same origin as the two principal bands of the ligand spectrum. In addition, the complexes also displayed a broad unstructured low intensity band centred at ~447-462nm assigned to ligand to metal charge transfer transitions (LMCT) charge transfer transition ($N\rightarrow Ni^{2+}$) which might have obscured the d-d bands.

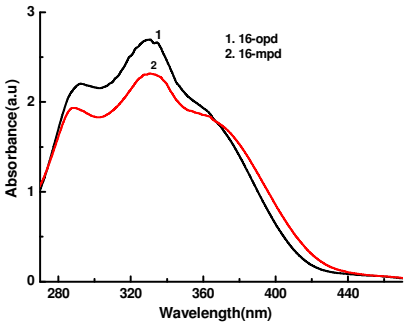

Fig. 1: Absorption spectra of the ligands.

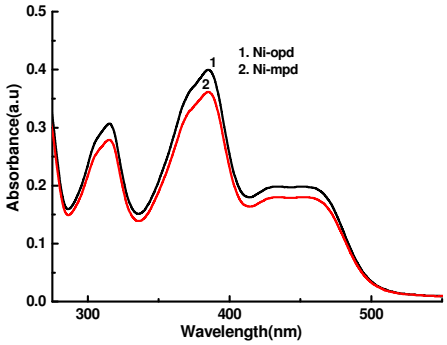

Fig. 2: Absorption spectra of the complexes.

The photoluminescence properties of the compounds were investigated in dichloromethane solution and in thin films at room temperature. The ligands are non-emissive, but their corresponding nickel(II) complexes displayed strong blue emission both in solution and solid state (**Fig.3**), usually observed in similar Schiff base metal complexes with the emission maximum centred at ~454-488nm originating from π-π* singlet ligand-centred excited state.[38-41] The emission maxima for typical compound Ni-16opd in solid state (~481nm, Φ = 7%) is considerably red shifted with respect to that recorded in solution (~456nm, Φ = 23%). In solid state after complexation, the free rotation of the flexible bonds of the ligand is reduced and hence energy dissipation through non-radiative channels decreases leading to shift of emission wavelength to lower energy. Moreover in the solid state, a larger electronic delocalization and intermolecular aromatic interaction leads to a lowering of energy of the electronic states.[38-41] The spectral data are summarized in Table 1.

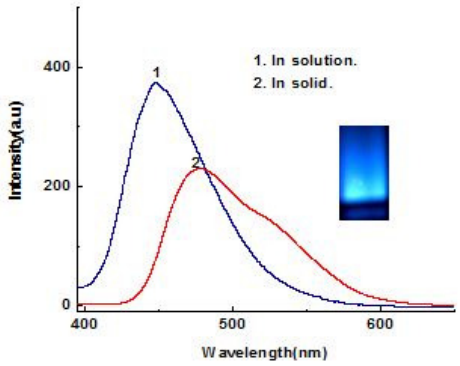

Fig. 3: Emission spectra of the Ni-16opd complex.

Table 1: UV-visible and photoluminescence data of the compounds.

Compounds	$\pi \rightarrow \pi^*$ (ε, l mol^{-1} cm^{-1})	LMCT (ε, l mol^{-1} cm^{-1})	PL[a] (Solution)	PL[a] (Solid)
16opd	292 nm (22000)	-	-	-
	329 nm (26800)			
	363 nm (18981)			
Ni-6opd	315 nm (2770)	447 nm (1800)	456 nm	481 nm
	385 nm (3610)			
16mpd	289 nm (19300)	-		
	330 nm (23100)			
	365 nm (18110)			
Ni-6mpd	314 nm (2200)	448 nm (1310)	454 nm	478 nm
	385 nm (2670)			

[a]: Photoluminescence data.

Thermal microscopy and differential scanning calorimetry study:

The thermal behaviour of the compounds (Table 2) was investigated by polarizing optical microscopy (POM) and differential scanning calorimetry (DSC) study. The ligands are found to be non-mesomorphic. However, on co-ordination to nickel(II) ion mesomorphism was induced, reflecting conformational rigidification of the ligand on complexation. Monotropic mesomorphism was encountered for Ni-16mpd complex. The Ni-16opd showed enantiotropic mesomorphic behaviour. Polarized optical microscopy of a representative complex (Ni-16opd) revealed that, upon cooling the sample from isotropic phase, a sphereulitic growth appeared which coalesce to a fan-like texture (**Fig. 4**) at ~130°C with large homeotropic regions, suggesting a columnar mesophase (Col). The mesophase is stable down to room temperature. The DSC thermogram (**Fig. 5**) for the complex (Ni-16opd) exhibited two transitions in heating and two in cooling cycle. The melting temperatures of the complexes showed a decreasing trend with X = H, CH_3 in that order (Table 2). Another interesting aspect is the quite low enthalpy values for the phase transitions in the unsubstituted complex (Ni-16opd) compared to those observed for the substituted one (Ni-16mpd). In general, complexes with higher molecular weights tend to exhibit larger enthalpy changes during mesophase to isotropic liquid transitions.[5] Relatively high enthalpies for mesophase transition to isotropic state in the substituted complex, Ni-16mpd could be indicative of the formation of a higher order columnar phase in this system.[42]

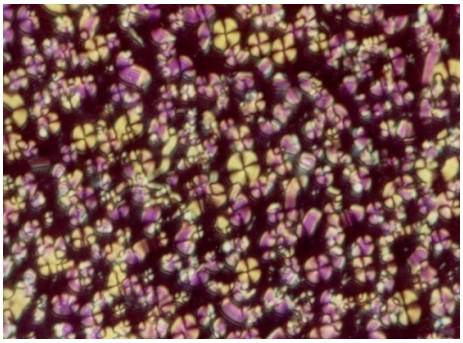

Fig. 4: POM texture of Ni-16opd complex.

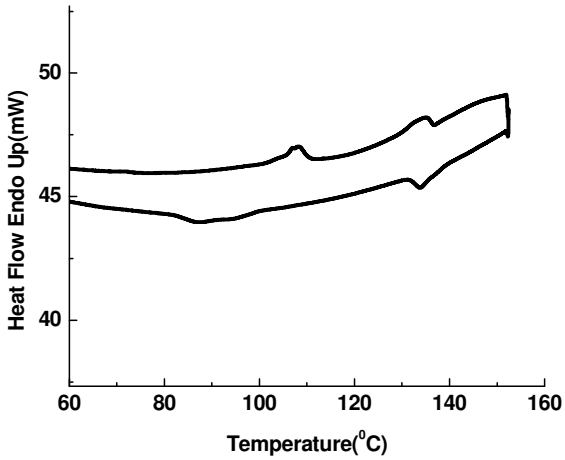

Fig. 5: DSC thermogram of Ni-16opd complex.

Table 2: POM and DSC data of the complexes.

Compounds	***T*** **(°C)**	**Transition**	**ΔH (kJmol^{-1})**
Ni-16opd	108.2(Heating)	Cr-Col$_r$	2.9
	135.0(Heating)	Col$_r$-I	2.6
	133.9(Cooling)	I-Col$_r$	2.5
	87.1(Cooling)	Col$_r$-Cr	0.93
Ni-16mpd	84.4(Heating)	Cr-Col$_r$	12.8
	125.2(Heating)	Col$_r$-I	12.9

XRD-study:

The mesophase structure was confirmed by temperature-dependent X-ray diffraction analysis (Table 3). The spectrum was recorded for a typical compound, Ni-16opd at 130°C. In the low angle region two fundamental sharp reflections were observed characteristic of a rectangular columnar mesophase (**Fig.6**). Further, there are two

diffuse reflections in the wide angle region. One corresponds to 4.9Å, for molten alkyl chains, the relatively sharper one at about 3.6 Å, well separated from the broad peak is due to the regular stacking of the molecules within the columnar mesophase. In the wide angle region the presence of another less broad peak at about 7.6Å may indicate the formation of dimers (**Fig.7**) along the axis of the column. Moreover, due to the absence of (21) peak in the XRD spectrum, the symmetry of the lattice can be further assigned to a *c2mm* plane group.[26,43] The lattice constants of this rectangular phase are a = 38.2Å and b = 15.4Å. The lattice parameter a = 38.2Å is larger than the radius of the half-disc shaped molecule (~20.6Å). Therefore, the hemi-disc molecules in the mesophase are believed to organize themselves in an anti-parallel fashion (**Fig.7**). A similar type of molecular self assembly was reported earlier.[19,44]

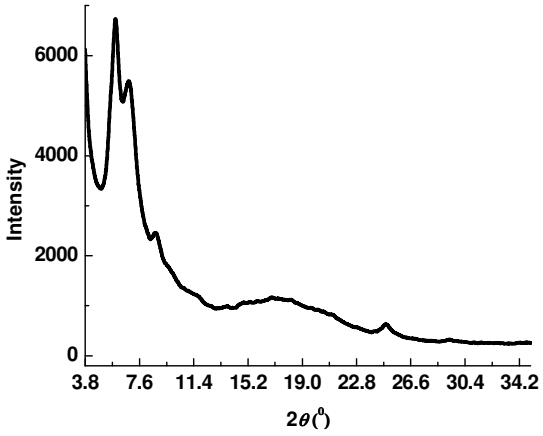

Fig. 6: XRD-pattern of Ni-16opd.

Table 3: XRD data of the Ni-16opd.

Compound	d_{obs}[Å][a]	d_{calc}[Å][b]	hk[c]	Parameters
Ni-16opd	19.3	19.2	20	Col_r- *c2mm*
	14.1	14.3	11	a=38.2Å
	10.3	10.4	31	b=15.4Å
	7.6			S=588.3Å^2
	4.9			V_m=1551Å^3
	3.5			h=2.1Å
				S_{col}=294.1

[a]d_{obs} and [b]d_{calc} are experimentally and theoretically measured diffraction spacings at 130°C. [hk][c] are indexation of the reflections. Mesophase parameters d, molecular

volume V_m is calculated using the formula:V_m=M/λρNA where M is the molecular weight of the compound, N_A is the Avogadro number , ρ is the volume mass (≈1 g cm^{-3}), and λ(T) is a temperature correction coefficient at the temperature of the experimerient (T).λ= VCH_2 (T_0)/VCH_2 (T), T_0=25C.VCH_2 (T)= 26.5616+0°.02023.T, h is the intermolecular repeating distance deduced directly from the measured molecular volume and the lattice area according to h=V_m/S. For the Col_r phase, the lattice parameters a and b are deduced from the mathematical expression: a=$2d_{20}$ and $1/d_{hk}=\sqrt{h^2/a^2+k^2/b^2}$, where a, b are the parameters of the Col_r phase, S is the lattice area, S_{col} is the columnar cross-section (S=ab, S_{col}=S/2).

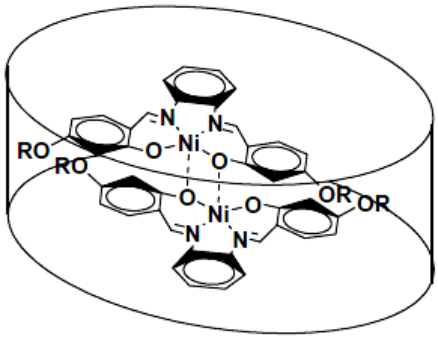

Fig. 7: Dimeric interaction of molecules

DFT study:

All the structures were completely optimized using the hybrid HF-DFT method, labelled as BLYP. The BLYP functional is comprised of a hybrid exchange functional as defined by Becke and the non-local Lee–Yang–Parr correlation functional.[45] We used DFT semicore pseudopotential with double numerical basis set plus polarization functions (DNP), which is comparable with the Gaussian 6-31G(d,p) basis set in size and quality.[46] All structures were relaxed without any symmetry constraints. Convergence in energy, force, and displacement was set as 10^{-5} Hartree (Ha), 0.001 Ha/Å, and 0.005Å, respectively. All calculations were performed with the DMol3 program package.[46-48]

Global hardness (η) of an electronic system is defined[49] as the second derivative of total energy (E) with respect to the number of electrons (N) at constant external potential, $\nu(\vec{r})$

$$\eta = \frac{1}{2}\left(\frac{\delta^2 E}{\delta N^2}\right)_{v(r)} = \left(\frac{\delta \mu}{\delta N}\right)_{v(\vec{r})}$$

Global softness is the inverse of global hardness with a factor of half

$$S = \frac{1}{2\eta} = \left(\frac{\delta^2 N}{\delta E^2}\right)_{v(\vec{r})} = \left(\frac{\delta N}{\delta \mu}\right)_{v(\vec{r})}$$

By applying finite difference approximation the global hardness and softness are expressed as:

$$\eta = \frac{IE - EA}{2}, \quad S = \frac{1}{IE - EA}$$

where IE and EA are the first vertical ionization energy and the electron affinity of the molecule, respectively. Using Koopmans' theorem IE and EA can be approximated as negative of E_{HOMO} and E_{LUMO}, respectively and thus Chemical hardness and Chemical softness can be written as

$\eta = \frac{E_{LUMO} - E_{HOMO}}{2}$ and $S = \frac{2}{E_{LUMO} - E_{HOMO}}$ respectively.[50]

The optimized structure of the complex is shown in (**Fig.8**). The complexes are neutral with Ni^{2+} in d^8-system. We optimized singlet and triplet state of the complexes and found singlet square planar geometry is more stable. The 3D isosurface plots of the lowest unoccupied molecular orbital (LUMO) and the highest occupied molecular orbital (HOMO) for the nickel complex (Ni-16opd) is shown in (**Fig.9** and **Fig.10**). In all the complexes, electron density of the HOMO is mainly localized in between Ni–O and Ni–N bonds, while the electron density of the LUMO is localized on nickel atoms. The Ni-O (apical) interaction in the dimer (**Fig.9** and **Fig.10**) expectedly occurs between molecular orbials of sigma (O) and pi*(Ni). The HOMO, LUMO energy difference of the complexes depends on the electronic nature of the substituents.[51-53] The energy differences decrease in the order of Ni-16mpd > Ni-16opd. The HOMO–LUMO energy separation can be used as a measure of kinetic stability of the molecule and could indicate the reactivity pattern of the molecule. A small HOMO–LUMO gap implies a low kinetic stability and high chemical reactivity, because it is energetically favourable to add electrons to LUMO or to extract electrons from a HOMO. We further calculated the chemical softness values for both model

complexes from their HOMO and LUMO energies. The chemical softness values of hydrogen and methyl-substituted complexes are 2.058 and 2.051 eV^{-1} respectively. Some of the selective geometric parameters of optimized hydrogen and methyl-substituted nickel complex, evaluated by DFT calculation at BLYP/DNP level are reported in Table 4. From DFT data, it is noticed that the complexes have an average Ni—O and Ni—N bond lengths are in the range of 1.93-1.92 and 2.00-1.99Å respectively. The average bond angles are in the range of 94.70-92.8 and 83.20-83.6 for O1–Ni–O2 and N1–Ni–N2 respectively around the nickel atom deviate substantially from the tetrahedral values indicating a distorted planar four coordinate geometry. The dihedral angles O(1)O(2)N(1)N(2) and N(1)O(1)O(2)N(2) as computed from DFT are found to lie in the range 15-20° (Table 4)reflecting the deviation from planarity. A strained conformation of the $[N_2O_2]$-donor tetradentate ligand with long pendant alkyl side chains is believed to have caused the deviation from planar symmetry. Moreover, a short rigid central spacer group in the present complexes presumably prevented the formation of a tetrahedral environment around nickel (II), leading to a distorted square planar geometry. The length of the complexes based on the fully extended structure is found to be ~40.7Å (measured from the two terminal end of the side alkyl chain).

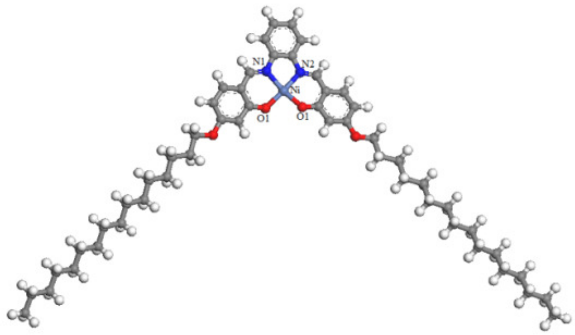

Fig.8: Optimized structure of Ni-16opd.

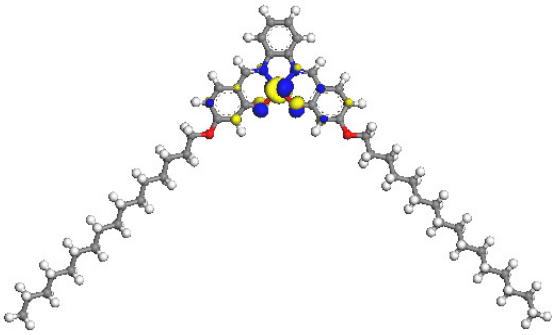

Fig. 9: LUMO of Ni-16opd.

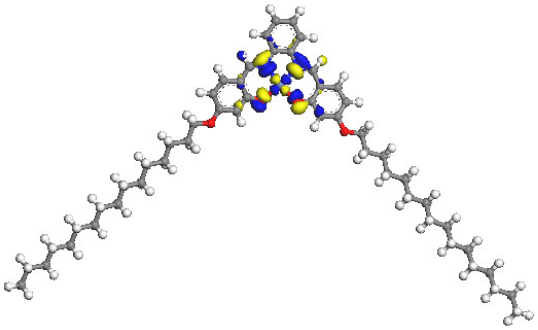

Fig. 10: HOMO of Ni-16opd.

Table 4: DFT data of the complexes. Bond lengths are reported in Å and bond angles in degrees.

Structure parameter	**Ni-opd**	**Ni-mpd**
Ni—O(1)	1.929	1.930
Ni—O(2)	1.930	1.931
Ni—N(1)	1.999	1.999
Ni—N(2)	1.999	2.001
O(1)—Ni—O(2)	94.67	94.58
N(1) —Ni—N(2)	83.16	83.20
N(1) —Ni—O(2)	165.14	165.65
O(1) —Ni—N(1)	92.76	92.71
O(1) —Ni—N(2)	165.29	165.45
N(2) —Ni—O(2)	92.63	92.58
HOMO in eV	-3.584	-3.542
LUMO in eV	-2.612	-2.567
ΔE in eV	0.972	0.975
Chemical Softness	2.058	2.051
O(1)O(2)N(2)N(1)	19.3	18.8
N(1)O(1)O(2)N(2)	17.9	17.5

4.2.2 Synthesis of oxovanadium(IV) salophen complex:

The synthesis of Schiff base ligands [(L = *N,N′*-bis-(4-(4′-n-alkoxy)-salicylidene) 4-Me-1,2-phenylenediamine), hereafter abbreviated as n-mpd, where n indicates the number of carbon atoms in alkyl chains, n = 14,16,18 and mpd = 4-methyl-1,2-phenylene diamine] were carried out as per procedure reported earlier.[14,15] A new series of mononuclear oxovanadium(IV) complexes of the type [VOL], L = N, N'-di-(4-*n*-alkoxysalicylidene)-4-Me-l,2-diamino-benzene (n = 14, 16, 18) have been synthesised and are presented in **Scheme 2**.

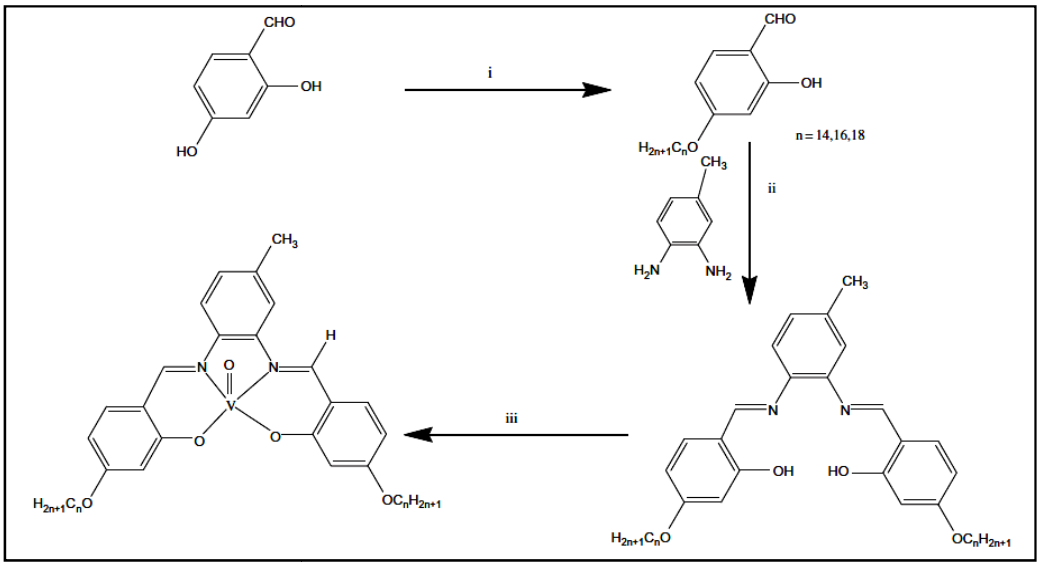

Scheme 2: i.$C_nH_{2n+1}Br$, $KHCO_3$, KI, dry acetone, Δ, 40h, and ii. glacial AcOH, absolute EtOH Δ, 4h iii.$VOSO_4.5H_2O$, MeOH, TEA. Δ, 1h

Synthesis of mononuclear oxovanadium(IV) complexes (VO-nmpd):

The ligand 18-mpd (0.086g, 0.1mmol) or 16-mpd (0.081g, 0.1mmol) or 14-mpd (0.075g, 0.1mmol) was dissolved in a minimum volume of absolute ethanol. An equimolar amount of vanadyl sulphate, $VOSO_4.5H_2O$ (0.02g, 0.1mmol) in methanol was then added slowly followed by the addition of triethylamine and refluxed for 2 h. A greenish yellow solid formed immediately. This was filtered, washed with diethyl ether and recrystallised from methanol/dichloromethane (1:1).

VO-18mpd:

Yield: 0.139g, 75%. FAB mass (m/e, fragment): m/z: calc. 931.61; found: 932.61[M+H^+]; Analysis calculated for $C_{57}H_{88}N_2O_5V$ (932.61): C, 73.44; H, 9.51; N

3.0. Found: C, 73.41; H, 9.52; N, 3.11%. IR (ν_{max}, cm^{-1}, KBr): 2920 ($\nu_{as(C-H),}$ CH_3), 2850 ($\nu_{s(C-H),}$ CH_3), 1612 ($\nu_{C=N}$), 981 ($\nu_{V=O}$).

VO-16mpd:

Yield: 0.126g, 70%. FAB mass (m/e, fragment): m/z: calc. 875.55; found: 876.55[M+H^+]; Analysis calculated for $C_{53}H_{80}N_2O_5V$ (876.55): C, 72.65; H, 9.20; N 3.20. Found: C, 72.64; H, 9.22; N, 3.21%. IR (ν_{max}, cm^{-1}, KBr): 2924 ($\nu_{as(C-H),}$ CH_3), 2852 ($\nu_{s(C-H),}$ CH3), 1611 ($\nu_{C=N}$), 982 ($\nu_{V=O}$).

VO-14mpd:

Yield: 0.131g, 75%. FAB mass (m/e, fragment): m/z: calculated 819.49; found: 820.49 [M+H+]; Analysis calculated for $C_{49}H_{72}N_2O_5V$ (820.49): C, 71.77; H, 8.85; N 3.42. Found: C, 71.75; H, 8.82; N, 3.41%. IR (ν_{max}, cm^{-1}, KBr): 2923 ($\nu_{as(C-H),}$ CH_3), 2851 ($\nu_{s(C-H),}$ CH_3), 1609 ($\nu_{C=N}$), 984 ($\nu_{V=O}$).

4.2.2.1 Results and discussion:

Synthesis and structural assessment:

Synthesis of the compounds was achieved through a facile and straightforward procedure as described in our earlier report.[14,15] The synthetic strategy for the ligands [(L=N,N-bis(4-(4-n-alkoxy)salicylidene)1,2-phenylenediamine), hereafter abbreviated as nmpd, where n indicates the number of carbon atoms in alkyl chains, n = 14, 16, 18 and mpd = 4-Me-1, 2-phenylenediamine] and the oxovanadium(IV) complexes (VO-nmpd) are presented in **Scheme 2**. The mononuclear oxovanadium(IV) complexes, VO-nmpd(n = 14,16,18), were prepared by the reaction of the appropriate ligand with vanadyl sulphate (1:1 molar ratio) and recrystallised from methanol/dichloromethane; the complexes were isolated as greenish yellow solids in good yields. The compounds were characterised by elemental analyses, Fourier transform infra-red (FT-IR) spectroscopy, ultraviolet–visible (UV-Vis) spectroscopy, ^1H nuclear magnetic resonance (NMR) and mass spectrometry. The analytical and spectral data of the compounds are in good agreement with the proposed formulae. A weak broad band in the region 3250-3350cm^{-1} due to a hydrogen bonded -OH group in the free Schiff base ligand was not observed in the IR spectra of the complexes, indicating that the phenolic oxygen is deprotonated and coordinated in the complexes. A strong ν(C=N) band appearing in the range 1612-1610cm^{-1} for the complexes is

considerably red shifted compared to that of the free Schiff base ligands (~1629cm^{-1}), indicating coordination of the azomethine nitrogen to the metal. Observation of the vanadyl(V=O) stretching mode at a relatively higher wave number (~980 cm^{-1}) is suggestive of the absence of any intermolecular (. . . V=O . . . V=O. . .) interaction, indicating the monomeric nature of the complexes.[54] Such linear chain interactions usually cause $\nu_{V=O}$ to shift to lower wave number (~870 cm^{-1}). ^{1}H NMR spectra of the ligands showed signals at δ = 13.4-13.8ppm and 8.5ppm, corresponding to the OH-proton and imine proton, respectively. The fast atom bombardment (FAB) mass spectra of the vanadyl(IV) complexes are concordant with their formula weights. The solution electrical conductivity of the complexes recorded in dichloromethane (10^{-3}M) was found to be < 10 Ω^{-1}cm^{-1}mol^{-1}, much lower than expected for a 1:1 electrolyte, thus confirming the non-electrolytic nature of the complex. The electronic absorption spectrum (**Fig.11**) of ligand 16-mpd showed two bands at ~290nm and ~325nm attributed, respectively, to a π-π* transition localised on the aromatic rings and a third intense peak at ~364nm for n-π* transition of the imine chromophore. Upon complexation with VO(IV), these bands are red shifted to a longer wavelength (Table 5). The complexes exhibited a strong band at ~400nm, due to a ligand-to-metal charge-transfer (LMCT) transition. A similar observation was noted for all other compounds (Table 5).

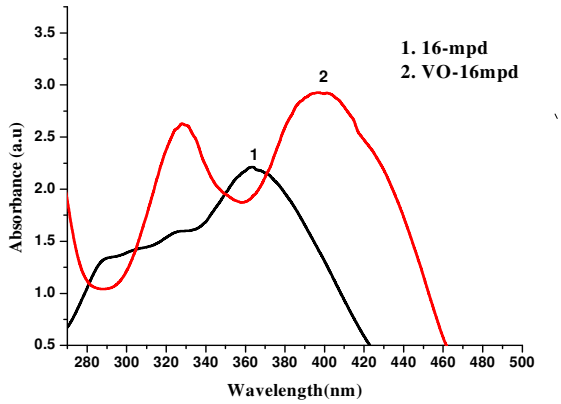

Fig.11: UV-visible spectra of 16-mpd and VO-16mpd.

Table 5: UV-visible spectral data of ligands (n-mpd) and complexes (VO-nmpd)

Compound	λ_{max}(nm)	
	$\pi \rightarrow \pi^*$ (ε, l mol^{-1} cm^{-1})	LMCT (ε, l mol^{-1} cm^{-1})
18-mpd	288 (13000)	-
	326 (15900)	
	364 (22400)	
VO-18mpd	325 (26300)	401(29100)
16-mpd	290 (12900)	-
	326 (15900)	
	362 (22200)	
VO-16mpd	326(26400)	400(29100)
14-mpd	290 (12900)	-
	334 (16000)	
	364 (22400)	
VO-14mpd	325 (26300)	402(29100)

Cyclovoltammetric Study:

The redox behaviour for a typical complex (VO-16mpd) was probed by cyclic voltammetry in dichloromethane solution in the potential range -1.0 to 1.4V versus saturated calomel electrode (SCE) at a scan rate of $0.05Vs^{-1}$. The voltammogram (**Fig.12**) displayed a quasi-reversible (peak separation ~82mV) one-electron response at (E_p^c =0.64V, E_p^a = 0.86V, E_p = 0.22V) assigned to a VO(V)/VO(IV) couple.

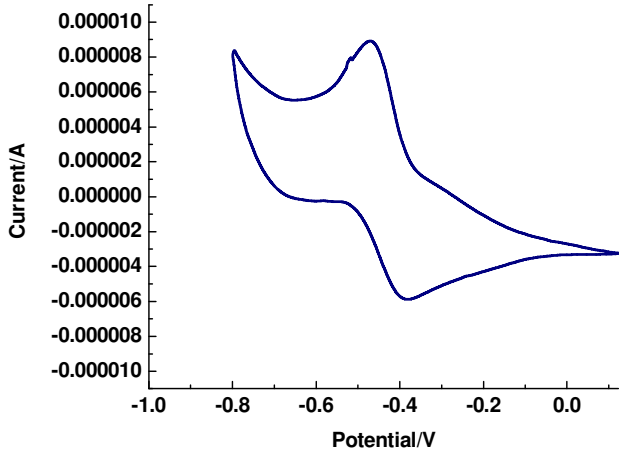

Fig. 12: Cyclic voltammogram of VO-16mpd

POM and DSC Study:

The mesomorphic behaviour of the complexes was investigated by polarising optical microscopy (POM) and differential scanning calorimetry (DSC). The ligands did not show liquid crystallinity, but the complexes exhibited enantiotropic columnar mesophases. Table 6 summarises the phase behaviour of these compounds. In the POM study, the sample transformed to the isotropic liquid at ~192°C. Upon cooling, a typical broken mosaic texture is observed at ~185°C (**Fig.13**). This is a very characteristic feature of rectangular columnar mesophase.On further cooling, the texture of this phase transformed to another pattern with focal conic texture at ~40°C. Interestingly, this optical texture remained unaltered till room temperature. The DSC traces obtained at a rate of 5°C min^{-1} (**Fig.13**) showed two transitions in the heating cycle and two in the cooling cycle. All the compounds possessed excellent thermal stability. The reversibility of the thermal behaviour was confirmed by DSC on subsequent heating-cooling runs. The formation of mesophases was dependent on the carbon length of terminal chains. The clearing temperatures slightly increased with a reduction in the carbon chain length of terminal alkoxy groups. The Col-I/I-Col phase transition enthalpy is found to be (~ΔH = 14.3-14.9kJmol^{-1}). The relatively high enthalpy value is ascribed to the increased mesophase order caused by rather large Vander Waal's interactions between the core groups of the neighbouring molecules in the two-dimensional (2D) rectangular mesophase relative to that of the one-dimensional (1D) mesophase. The columnar phase transformation from one rectangular type (Col_{r1}) to another (Col_{r2}), as observed in the POM and DSC study, was confirmed by the powder X-ray diffraction (PXRD) study. It is argued that this behaviour originated from an increase in the intercolumnar distance concomitant with closer packing of the discs within the same column. The Col_{r1} mesophase formed showed marked stability and did not crystallise even at room temperature, as evidenced by DSC and POM study. Such columnar phase transformation behaviour between two rectangular columnar mesophase is uncommon but not unprecedented.[55] The mesomorphic properties of such 'salphen' type complexes appear to be strongly dependent on the aromatic spacer and metal ions. In earlier reports, we found that the analogous oxovanadium complexes without any substituent in the aromatic spacer group showed lamellar columnar mesomorphism.[17]

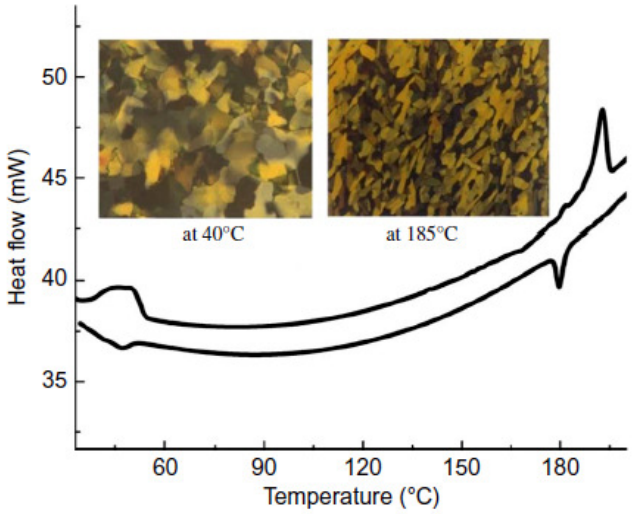

Fig. 13: Combined DSC curve and POM texture of VO-16mpd.

Table 6: DSC data of the complexes.

Compounds	Heating (ΔH, kJmol^{-1})	Cooling (ΔH, kJmol^{-1})
VO-18mpd	Col_{r1} 50.3(14.3) Col_{r2} 193.0(14.9) I	I179.6(14.7)Col_{r2}46.7(14.1) Col_{r1}
VO-16mpd	Col_{r1} 54.5(13.9) Col_{r2} 194.3(14.7) I	I184.7(14.1)Col_{r2}49.3(13.8) Col_{r1}
VO-14mpd	Col_{r1} 56.7(14.4) Col_{r2} 196.0(14.6) I	I189.6(14.3)Col_{r2}52.1(14.4) Col_{r1}

PXRD Study:

The mesophase structures were also confirmed by variable temperature powder XRD experiments, performed on a representative compound VO-16mpd (Table 7). At 40°C, in the small-angle region, several sharp Bragg reflections were observed (**Fig.14)** which could be indexed to rectangular 2D lattices of the Col_r phase.[56] In the wide angle region, diffuse reflections corresponding to a spacing of ~4.5Å can be attributed to the average distance between the liquid-like (molten) aliphatic side chains. A less intense peak at ca.7.1Å indicates dimeric interaction of the hemi-disc shaped molecules along the columnar axis. Quite a different diffractogram (**Fig.15**) is obtained for VO-16mpd at 190°C. In this case, two fundamental sharp reflections were observed in the low angle region which can be indexed as the (20) and (11) reflections of a rectangular lattice. Scattering centred on 4.5Å in the wide angle region relates to the liquid-like order of the peripheral tails. Notably in both cases, in the

absence of any hk pairs with h + k = 2n + 1, the symmetry of the lattice can be further assigned to a *c2mm* plane group.[56] Moreover the XRD pattern did not show any reflections around 3.0-3.5Å, clearly suggesting lack of any kind of long-range order between molecules due to π-π intermolecular interactions within the columns. The lattice constant 'a' in both cases is larger than the radius of the half disc so the two half disc molecules organise themselves in head-to-head fashion to form a discoid shell (**Fig.16**). This observation, coupled with the findings of the POM and DSC study, clearly confirmed the existence of two rectangular columnar phases.

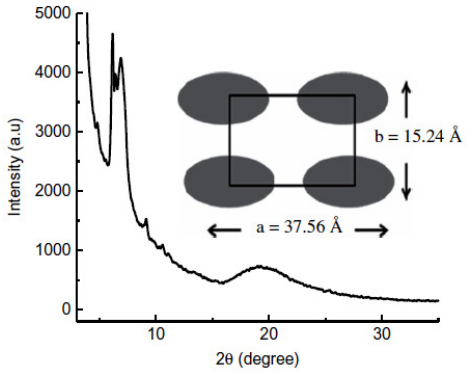

Fig. 14: XRD pattern of VO-16mpd at 40°C

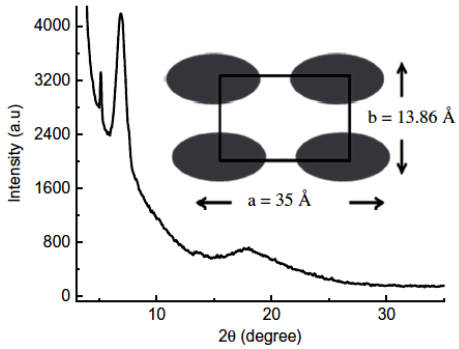

Fig. 15: XRD pattern of VO-16mpd at 190°C

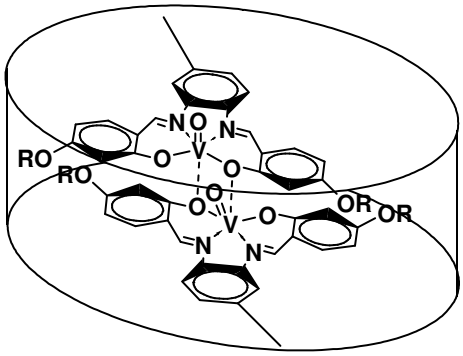

Fig. 16: Dimeric interactions of the half disc shaped molecules in the column

Table 7: XRD data of VO-16mpd.

Compound	d_{obs}[Å][a]	d_{calc}[Å][b]	hk[c]	Parameters
VO-16mpd at 40°C	18.78	18.76	20	a = 37.56 Å
	14.12	14.14	11	b = 15.24 Å
	13.05	13.07	31	S = 572.41 $Å^2$
	9.71	9.73	40	S_{col} = 286.20
	7.13	7.15		V_m = 1663.49 A^3
	4.51	4.53		-
VO-16mpd at 190°C	17.50	17.52	20	a=35Å, b=13.86 Å
	12.83	12.82	11	S = 485.1 $Å^2$
	6.52	6.54		S_{col} = 242.55
	4.96	4.97		V_m = 1483.05 $Å^3$

[a]d_{obs} and [b]d_{calc} are experimentally and theoretically measured diffraction spacings at 194°C and 40°C. [hk][c] are indexation of the reflections. Mesophase parameters d, molecular volume V_m is calculated using the formula: $V_m=M/\lambda\rho NA$ where M is the molecular weight of the compound, N_A is the Avogadro number, ρ is the volume mass (≈1 g cm^{-3}), and λ(T) is a temperature correction coefficient at the temperature of the experimerient(T). λ= VCH_2 (T_0)/VCH_2 (T), T_0=25°C.VCH_2 (T)= 26.5616+0.02023.T, h is the intermolecular repeating distance deduced directly from the measured molecular volume and the lattice area according to $h=V_m/S$. For the Col_r phase, the lattice parameters a and b are deduced from the mathematical expression: $a=2d_{20}$ and $1/d_{hk}=\sqrt{h^2/a^2+k^2/b^2}$, where a, b are the parameters of the Col_r phase, S is the lattice area, S_{col} is the columnar cross-section (S=ab, S_{col}=S/2).

DFT Study:

Despite several efforts, an X-ray quality single crystal could not been grown, so density functional theory (DFT) studies were undertaken to ascertain the optimized geometry of the VO-16mpd complex molecule (**Fig.17**). The ground state geometries in the gas phase of the complex were fully optimised using the unrestricted BLYP/DNP methods without imposing any symmetry constrain. The BLYP functional, used throughout this study, comprises of a hybrid exchange functional as defined by Becke and the non-local Lee–Yang–Parr correlation functional.[45-48] The basis set chosen is DNP, the double numerical atomic orbitals augmented by polarisation functions. Relativistic effects were taken into account with an all-electron scalar relativistic method based on the Douglas–Kroll–Hess (DKH) transformation. All calculations were performed with the DMol3 program package. It has been found that the average V–O and V–N bond lengths are 2.0 and 2.1Å, respectively, which matched quite well with the other related vanadium salphen complexes.[17] The bond angles 86.79° and 86.85° for O–V–O and N–V–N, respectively, revealed a distorted square pyramidal geometry around the vanadyl centre. Highest occupied molecular orbital (HOMO) and lowest unoccupied molecular orbital (LUMO) diagrams of the complex are shown in **Fig.18** and **Fig.19**. The HOMO and LUMO energies of the complex are calculated to be -4.9eV and -3.1eV, respectively, ΔE = 1.8eV. The electron density of the LUMO is scattered over the C–N bonds and the phenyl rings of the ligand, while the HOMO is localised primarily on the vanadyl centre. Some of the selective geometric parameters of the optimised complex, VO-16mpd are shown in Table 8.

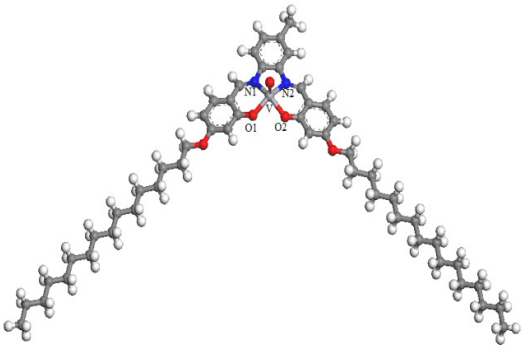

Fig. 17: Optimized structure of VO-16mpd

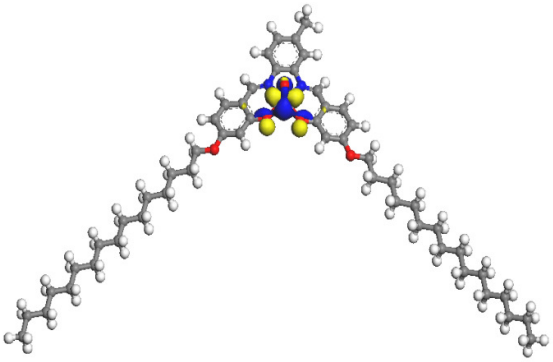

Fig. 18: HOMO of VO-16mpd

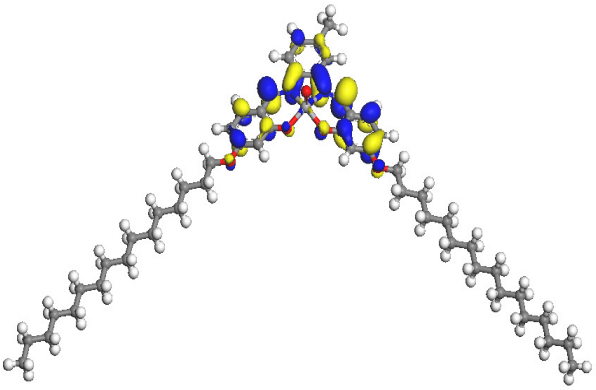

Fig. 19: LUMO of VO-16mpd

Table 8: Selected bond length and bond angles of VO-16mpd from DFT study.

Structure parameter	Distance(Å)/angles(°)
V-N	2.1
V-O	1.9
V=O	1.6
N-V-O	86.8
O-V-O	86.7
N-V-N	76.7

4.2.3 Synthesis of copper(II) complex with/without substituent in spacer group:

The synthesis of Schiff base ligands (16-opd/16-mpd) were carried out by condensation of 4-alkoxysubstituted aldehyde with unsubstituted/methyl-substituted 1,2-phenylene diamine as per procedure reported earlier.[14,15] The novel four-

coordinate copper(II) complexes (Cu-16opd/Cu-16mpd) were prepared by the reaction of appropriate ligand with copper acetate (1:1 molar ratio) in methanol are presented in **Scheme3**.

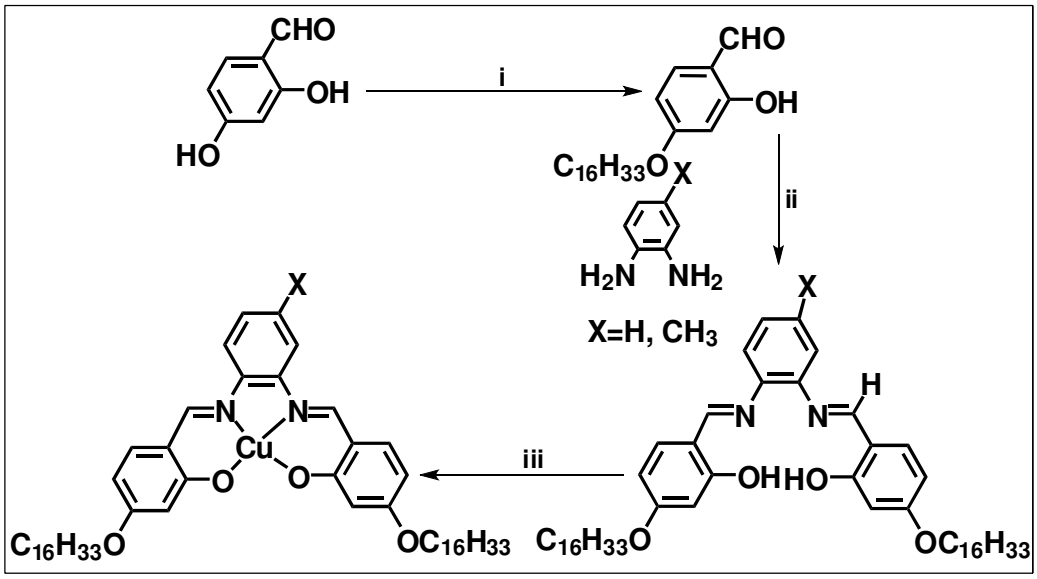

Scheme 3: i. $C_nH_{2n+1}Br$, $KHCO_3$, KI, dry acetone, Δ, 40h, and ii. glacial AcOH, absolute MeOH, Δ, 4h iii. $Cu(OAc)_2$. $2H_2O$, MeOH, stir, 1h.

Synthesis of copper (II) complexes:

The ligand 16-opd (0.079 g, 0.1 mmol) or 16-mpd (0.081 g, 0.1 mmol) was dissolved in minimum volume of absolute methanol. To this, an equimolar amount of copper acetate $Cu(OAc)_2.2H_2O$ (0.019g, 0.1mmol) in methanol was then added slowly and stirred for 2h at room temperature. A brown solid formed immediately was filtered, washed with diethyl ether and recrystallised from dichloromethane-methanol (1:1).

Cu-16opd:

Yield = 0.073g, 75%. FAB Mass (m/e, fragment): m/z: calc. 857.5; found: 858.5 [M + H^+]; Anal. Calc. For $C_{52}H_{78}N_2O_4Cu$: C, 72.7; H, 9.2; N 3.26. Found: C, 72.72; H, 9.1; N, 3.2%. IR (ν_{max}, cm^{-1}, KBr): 2921 ($\nu_{as(C-H),}$ CH_3), 2860 ($\nu_{s(C-H),}$ CH_3), 2848 ($\nu_{as(C-H)}$, CH_2), 1611 ($\nu_{C=N}$).

Cu-16mpd:

Yield = 0.065g, 65%. FAB Mass (m/e, fragment): m/z: calc. 871.5; found: 872.5 [M + H^+]; Anal. Calc. For $C_{53}H_{80}N_2O_4Cu$: C, 72.9; H, 9.2; N 3.2. Found: C, 73; H, 9.3; N,

3.1%. IR (νmax, cm^{-1}, KBr): 2921 ($\nu_{as(C-H),}$ CH_3), 2860 ($\nu_{s(C-H),}$ CH_3), 2848 ($\nu_{as(C-H),}$ CH_2), 1613 ($\nu_{C=N}$).

4.2.3.1 Results and discussion:

Synthesis and structural assessment:

The synthesis of Schiff base ligands (16-opd/16-mpd) by condensation of 4-alkoxysubstituted aldehyde with the 1,2-phenylene diamine and substituted 1,2-phenylene diamine are described in our earlier report.[14,15] The complexes (Cu-16opd/Cu-16mpd), were prepared by the reaction of appropriate ligand with copper acetate (1:1 molar ratio) in methanol (**Scheme 3**). Isolated as brown coloured solids in good yields, the complexes were recrystallised from methanol/dicholoromethane. The compounds were characterised by elemental analyses, ^1H and ^{13}C NMR (ligands only), Fourier transform infrared spectroscopy and ultraviolet-visible spectroscopy. From the infrared spectra, it was observed that the position of $\nu_{C=N}$ band of the free ligands appeared at 1610-1621cm^{-1}, which shifted to lower frequencies at 1603-1606cm^{-1}, respectively, upon complexation indicating azomethine nitrogen coordination with the metal. Moreover, absence of ν_{OH} mode of the ligands in the spectra of copper complexes further attests the coordination of phenolate oxygen atom to the metal ion. The fast atom bombardment (FAB)-mass spectra of the compounds matched well with their formula weights. Solution electrical conductivity of complexes recorded in dichloromethane (10^{-3}M) was found to be <10$\Omega^{-1}cm^{-1}mol^{-1}$, much lower than is expected for a 1:1 electrolyte, thus confirming the non-electrolytic nature of the complexes. The NMR spectra of ligands are described in our earlier reports.[14,15]

UV-Visible study:

The electronic spectra of compounds were recorded in dichloromethane solution (Table 9). The absorption spectra of Schiff base ligands are described in our earlier report.[14,15] In copper complexes the absorption bands appearing at ~265, ~319, ~350 and ~398nm are attributed to the intraligand π-π* electronic transitions (**Fig.20**). In comparison to the free ligands, the absorption maxima undergoes a red shift in the complexes may be due to the metal-perturbed ligand centred transition. In addition, a

weak band appeared as shoulder at ~420nm in the complexes which may have arisen due to Jahn-Teller distortion in copper (d^9) system.[57]

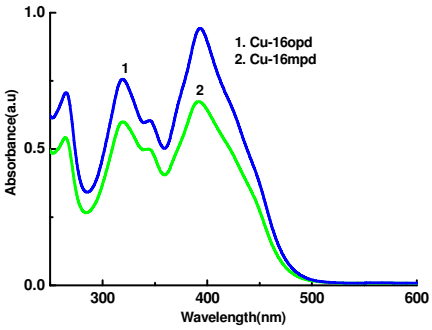

Fig. 20: Absorption spectra of complexes (dichloromethane; 10^{-5}M)

Table 9: UV-visible spectral data of ligands and copper complexes

Compound	λ_{max}(nm) $\pi \rightarrow \pi^*$ (ε, l mol^{-1} cm^{-1})	LMCT (ε, l mol^{-1} cm^{-1})
16-opd	292 (22000)	-
	329 (26800)	
	363 (18981)	
Cu-16opd	265 (69944)	422 (67865)
	320 (76966)	
	345 (61235)	
	393 (94832)	
16-mpd	289 (19300)	-
	330 (23100)	
	365 (18110)	
Cu-16mpd	264(54213)	420 (55955)
	320 (60842)	
	344 (50730)	
	392 (68202)	

Mesomorphic properties: POM and DSC study:

The liquid crystalline properties of the complexes were investigated by polarised optical microscopy (POM), differential scanning calorimetry (DSC) and X-ray diffraction (XRD) technique. The thermal data are summarised in Table 10. The ligands are found to be non-mesomorphic. However, the complexes Cu-16opd and

Cu-16mpd showed columnar mesomorphism. The tetrahedral methyl substituent in the spacer forces the neighbouring molecules above and below the plane sustaining weak intermolecular interactions. In POM study, upon cooling the sample from isotropic melt in particular, the complex Cu-16opd showed a typical mosaic texture (**Fig.21**) at ~100°C.The mesophase was later confirmed to be rectangular plastic columnar, Colrp by XRD study. In DSC experiments, three transitions both in heating and cooling cycle were observed for the complex (**Fig.22)**. The crystal to crystal transition observed at 53.7°C, could not be detected in POM study. Due to high viscous nature of the compound, a pronounced hysteresis in transition temperature is observed. High enthalpy values from isotropic to mesophase and vice versa clearly suggested that the mesophase is highly ordered. For Cu-16mpd, a typical broken fan-like texture (**Fig.23**) with some homeotropic region is formed on cooling from the isotropic liquid phase. In DSC (**Fig.24**) two peaks each for exothermic and endothermic transitions were found with low enthalpies, we have no suitable explanation for this behaviour at the moment. Temperature-dependent XRD studies were carried out for the Cu-16opd and Cu-16mpd complexes to confirm the mesophases. The PXRD data is summarised in Table 11. The powder X-ray diffraction (PXRD) pattern for Cu-16opd at 130°C in the low angle region consists of numbers of multiple peaks (**Fig.25**). In the wide angle region, a diffuse peak is observed at 4.3 Å with a rather narrow width indicating partial melting of the aliphatic arms. The most important feature is the presence of twin peaks at $2\theta \sim 20°$ and a sharp peak in the wide angle region generally observed in columnar plastic phase.[58] Occurrence of columnar plastic phase, denoted as Col_p, has been identified recently in discotic liquid crystals. The motional freedom of discs around the columnar axis in plastic phase is restricted.[59] The spacings of the first three reflections can be indexed to a rectangular lattice. For Cu-16mpd complex, in the small-angle region, a series of sharp Bragg peaks were present (**Fig.26).** The first two fundamental reflections can be indexed as the 11 and 20 reflections of a 2D rectangular lattice. Moreover, absence of any reflections with hk pairs ($h + k=2n + 1$) in the diffractogram, suggest the mesophase symmetry to be *c2mm* plane group. Furthermore, a diffuse reflection at 4.8Å in the wide angle region confirms the liquid like nature of the molten alkyl chain.[56] If the arbitrarily considered periodicity (h) along the column and the average

thickness of the molecular equivalents corresponding to the signal in the diffractogram is in the range of 10 to 13Å, the dimeric interaction is expected to be preserved in the mesophase.[60,61] The reflection at 10.33Å for Cu-16opd and at 11.49Å for Cu-16mpd conveys the periodicity for the existence of dimeric interaction between the half-disc shaped molecules. This is also indicated from the less broad peak at ~7.6Å in the wide angle region for both Cu-16opd and Cu-16mpd. For a corresponding average thickness along the column chosen arbitrarily for comparison sake and from measured molecular volume, the two complexes form a dimer per periodic stack of the columnar cross-section and four molecules (i.e. two dimers) pave the surface area of the rectangular lattice to make a repeating rectangular cell of ~10Å thick (**Fig.27**)**.** The radius of the semi-disc shaped molecule (~20.2Å) as computed from density functional theory (DFT) study is almost half the lattice spacing (a = 38.04Å) for Cu-16opd suggesting a face to face 'anti-parallel' assembly of the hemi-disc molecules in the columnar mesophase.

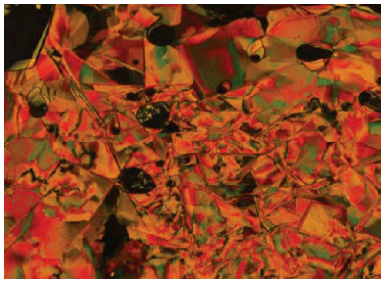

Fig. 21: POM texture of Cu-16opd complex at 100°C (20X magnification)

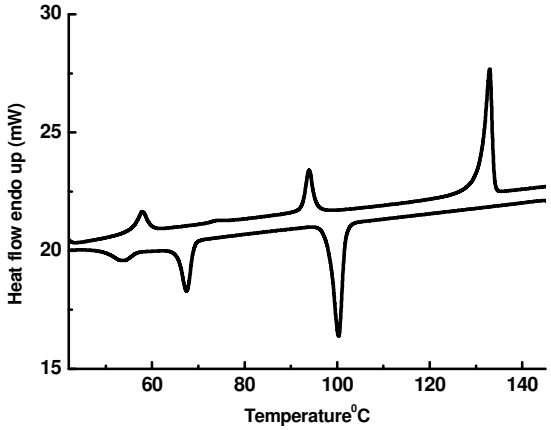

Fig. 22: DSC thermogram of Cu-16opd complex at 10°C min^{-1} (N_2 atmosphere)

Fig. 23: POM texture of Cu-16mpd complex at 152°C (10X magnification)

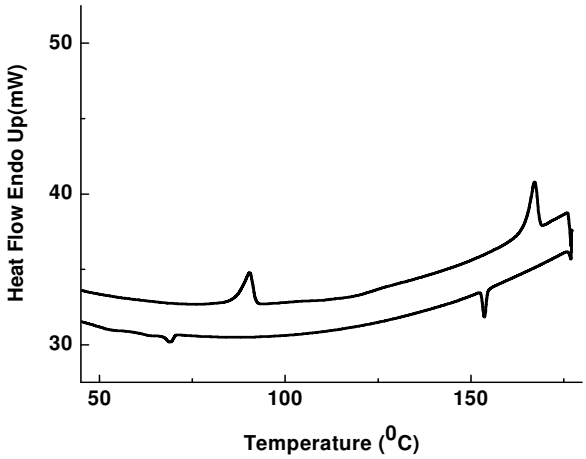

Fig. 24: DSC thermogram of Cu-16mpd complex at 10°C min^{-1} (N_2 atmosphere)

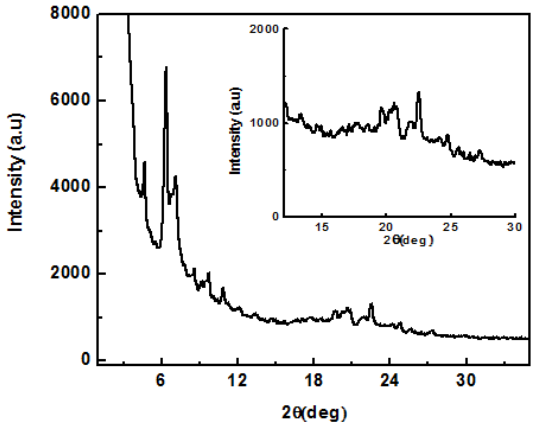

Fig. 25: XRD pattern of Cu-16opd complex at 130°C.

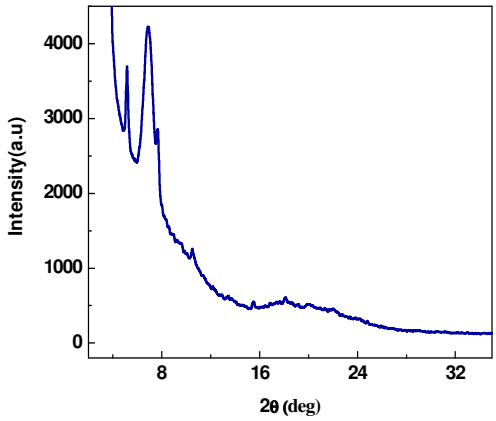

Fig. 26: XRD pattern of Cu-16mpd complex at 160°C.

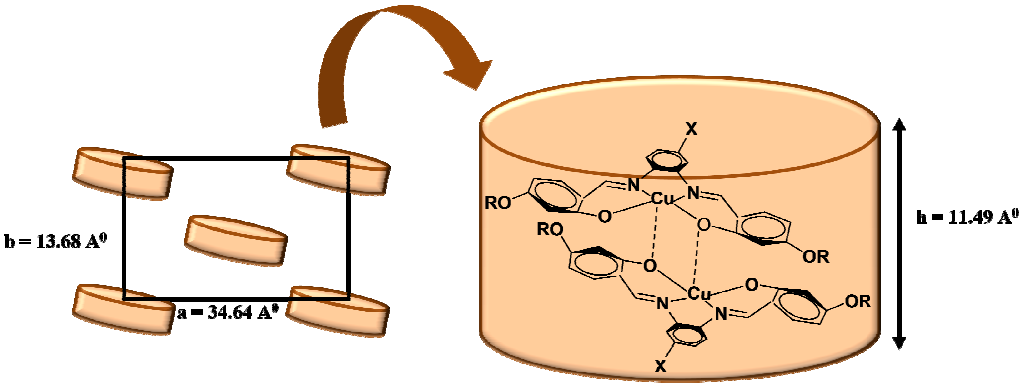

Fig. 27: Dimeric interactions of the half disc shaped molecules forming a disc-like shape.

Table 10: Transition temperature (°C), enthalpy (kJmol^{-1}) of compounds according to the DSC measurements.

Compounds	Transition	Peak Temperature	Enthalpy(ΔH, kJmol^{-1})
Cu-16opd	Cr-Cr_1	57.8	3.2
	Cr_1-Col_{rp}	93.9	6.0
	Col_{rp}-I	132.9	22.4
	I-Colrp	100.2	23.8
	Col_{rp}-Cr	67.5	8.5
	Cr-Cr_1	53.7	2.6
Cu-16mpd	Cr-Col_r	90.4	13.9
	Col_r-I	165.7	12.7
	I-Col_r	152.6	11.6
	Col_r-Cr	69.4	2.5

Table 11: XRD data of copper complexes

Compound	d_{obs}(Å)[a]	d_{calc}(Å)[b]	hk[c]	Parameters
Cu-16opd	19.01	19.02	20	Colrp
	13.91	13.92	11	a= 38.04Å
	12.41	12.43	31	b= 15.05Å
	10.33	10.32	40	S= 572.20Å2
	9.11	9.12	01	Vm= 1573.44Å^3
	8.19	8.18	42	N = 4
	7.6	7.5		h=10.33
	4.32	4.31	-	Scol = 86.10Å^2
Cu-16mpd	17.32	17.31	20	Colr - *c2mm*
	12.72	12.73	11	a=34.64 Å
	11.49	11.48	31	b=13.68 Å
	8.41	8.42	40	S=473.87 Å2
	7.5	7.4		
	6.44	6.45	-	Vm=1685.76 Å^3
	5.72	5.73		N = 4
	4.87	4.88		h=11.49
				Scol= 236.93Å^2

[a]d_{obs} and [b]d_{calc} are experimentally and theoretically measured diffraction spacings. [hk][c] are indexation of the reflections. Mesophase parameters d, molecular volume V_m is calculated using the formula: $V_m = M/\lambda\rho N_A$ where M is the molecular weight of the compound, N_A is the Avogadro number, ρ is the volume mass (≈1 g cm^{-3}) and λ(T) is a temperature correction coefficient at the temperature of the experiment (T). $\lambda = V_{CH2}(T°)/V_{CH2}(T)$, T° = 25°C. $V_{CH2}(T) = 26.5616 + 0.02023.T$. For the Col_r phase, the lattice parameters a and b are deduced from the mathematical expression: $a = 2d_{20}$ and $1/d_{hk} = \sqrt{h^2/a^2+k^2/b^2}$, where a, b are the parameters of the Col_r phase, S is the lattice area, S_{col} is the columnar cross-section (S = ab, S_{col} = S/2). The repeating columnar unit h is related to the molecular volume and the cross-section columnar area by the relationship $N\times V_{mol}/S$, where N is the number of molecular equivalent per repeat unit (in this case, to maintain the density along the column constant, N must be an integer or half-integer). Number of dimers constituting the rectangular disk, $N_D = N/2$

DFT study:

DFT has become a readily available tool which allows considerable insight into the nature and electronic structures of transition metal complexes. The geometrical optimizations of all the copper complexes were performed using Becke's three-

parameter non-local hybrid exchange potential and the nonlocal correlation functional of Lee, Yang, and Parr (B3LYP) with the 6-31G (d) basis set for all atoms except for copper, which has been described by the effective core potential of Wadt and Hay (Los Alamos ECP) included in the LanL2DZ basis set. The gas phase ground state geometries of the copper complexes were fully optimized using the unrestricted B3LYP methods without imposing any symmetry constrain with tight convergence criteria. Appropriate structures were confirmed as energy minima by calculating the vibrational frequencies using second derivative analytic methods, and confirming the absence of any imaginary frequencies. For Cu^{2+} complexes, which are open-shell systems, the expectation value showed that the spin contamination of the unrestricted wave function was always very small. All DFT calculations were carried out with the Gaussian 09 programs.[62] Natural charges were obtained from the natural bond orbital (NBO) population analysis. Some of the significant geometric parameters of the optimised hydrogen-, methyl- and nitro-substituted copper complexes, evaluated by DFT calculation at B3LYP level are displayed in Table 12. The complexes have an average Cu–O and Cu–N bond lengths in the range of 1.911-1.916 and 1.986-1.993 Å, respectively. The average bond angles arein the range of 89.8-89.9° and 83.1-83.2° for O1–Cu–O2 and N1–Cu–N2, respectively, while, O1–Cu–N2 and O2–Cu–N2 bond angles are calculated to be 176.5-176.6° and 176.4-176.6°, respectively, around the copper atom indicating slight distortion of square planar geometry (**Fig.28**). The dihedral angles O(1)O(2)N(1)N(2) and N(1)O(1)O(2)N(2) as computed from DFT are found to lie in the range 1.18-1.30° (Table 12) reflecting slight deviation from planarity. A strained conformation of the $[N_2O_2]$-donor tetradentate ligand with long pendant alkyl side chains is believed to have caused little deviation from planar symmetry. The molecular length of the complexes based on the fully extended structure is found to be around 42.76Å (measured from the two terminal end of the side alkyl chain), indicating no substituent effect on the molecular length. The optimized geometry also revealed that the oxygen and aromatic carbon (O–Car) distance increases from 1.271 in free ligand to 1.292 Å on complexation with copper. The O–Car bond is weakened upon formation of complex, implying that oxygen atom acts as a donor atom. DFT has emerged as a practical and effective computational tool with which electronic structure of transition metal complexes can be studied easily.

DFT with NBO analysis allows considerable insight into the nature of metal–ligand bonding. The natural charges and electronic configuration of the atoms of the complexes and free ligand evaluated by NBO analysis are summarised in Table 13. The calculated natural charges on the copper ions are considerably lower than the formal charge, +2. The electronic population on p_x, p_y and p_z orbitals of copper atom in its hydrogen- and -methyl substituted ligands are found to be (0.1186, 0.1164 and 0.0937) and (0.1186, 0.1145 and 0.0910) respectively. However, occupancy at the d_{xy}, d_{xz}, d_{yz}, $d_{x^2-y^2}$ and d_{z^2} orbitals of copper atoms in their complexes with hydrogen and methyl containing ligands are (1.4205, 1.9964, 1.9846, 1.9960 and 1.9686) and (1.4328, 1.9948, 1.9838, 1.9957 and 1.9712) respectively. All the d-orbitals are occupied by more than 1.96 e^- except the dxy (~1.42 e^-) orbitals. Comparing the atomic charges in the free ligands and their complexes with copper, it can be seen that the atomic charge redistribution occur on all the atoms in the complexes. The calculated natural atomic charges on copper atoms in its complexes with hydrogen- and methyl-substituted ligands are found to be +0.964 and +0.963 respectively, attesting ligand-to-metal charge transfer in all the complexes. According to the NBO analysis, the electronic configuration of Cu in Cu-16opd complex is: [core]$4s^{0.34}3d^{9.37}$ $4p^{0.33}$, which corresponds to 18 core electrons, 9.71 valence electrons (on 4s and 3d atomic orbitals) and 0.33 Rydberg electrons (mainly on 4porbital) give the 28.04 electrons. This is consistent with the calculated natural atomic charge on copper atom (+0.968e) in Cu-16opd complex. The natural atomic charge on oxygen atoms of the ligands hardly changes on complexation with copper ion. However, while, the atomic charges on nitrogen atom of the ligands changes significantly on complexation from -0.436 and -0.436 to -0.571 and -0.571, -0.436 and -0.434 to -0.573 and -0.573 respectively on complexation of hydrogen- and methyl- containing ligands with copper ions (Table 13). Frontier molecular orbital plays an important role in determining the electronic properties of molecules.[63] Lowest unoccupied molecular orbital (LUMO) and highest occupied molecular orbital (HOMO) energies of the complexes with 16-opd and 16-mpd are calculated to be -1.785eV and -5.261eV, -1.847eV and -5.161eV, respectively. The corresponding energy differences (ΔE) of the complexes are found to be 3.476eV and 3.314eV, respectively. The LUMO and HOMO energy as well as their energy differences of the complexes depend on the

electronic nature of the substituents. The energy differences decrease in the order of 16-opd > 16-mpd. The HOMO–LUMO energy differences evaluated from the lowest energy UV-Vis band for Cu-16opd and Cu-16mpd is 2.93eV and 2.96eV respectively, are somewhat lower than that obtained from DFT studies. This can be accounted by considering extensive intermolecular interactions in the solution phase (UV-Vis study) in comparison to free gaseous molecule in DFT study. A low HOMO–LUMO energy gap implies a low kinetic stability and high chemical reactivity, because it is energetically favourable to add electrons to LUMO or to extract electrons from a HOMO. We further calculated the chemical hardness values of hydrogen- and methyl-substituted copper complexes from their LUMO and HOMO energy difference. The chemical hardness values of hydrogen- and methyl- substituted complexes are found to be 1.738 and 1.657eV, respectively. According to maximum hardness principle[49] higher hardness value indicates higher stability.

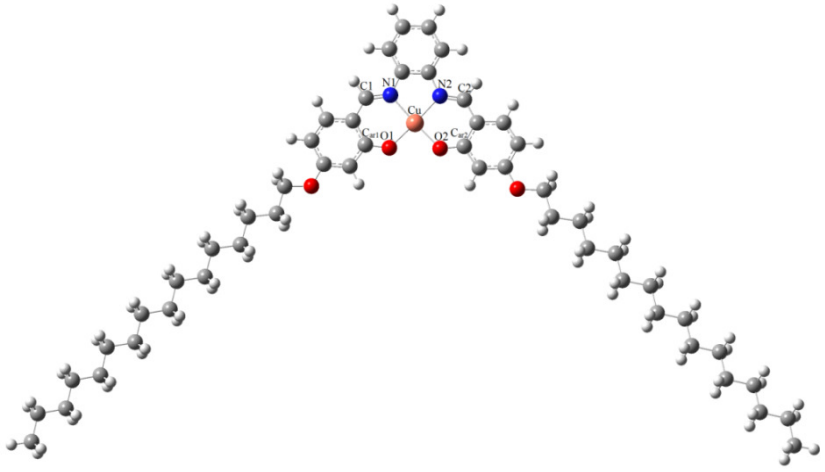

Fig. 28: Optimized structure of Cu-16opd

Table 12: Selected bond lengths (Å) and bond angles (°) and other related parameters of Cu(II) complexes evaluated at B3LYP level.

Structure parameters	Cu-16opd	Cu-16mpd
Cu—O1	1.915	1.915
Cu—O2	1.914	1.914
Cu—N1	1.991	1.992
Cu—N2	1.991	1.990
C1—N1	1.313	1.313
C2—N2	1.313	1.313
C_{AR1}—O1	1.291	1.292
C_{AR2}—O2	1.291	1.292
O1—Cu—O2	89.8	89.8
N1—Cu—N2	83.2	83.2
O1—Cu—N1	93.6	93.5
O2—Cu—N2	93.6	93.5
O1—Cu—N2	176.6	176.6
O2—Cu—N1	176.6	176.6
O(1)O(2)N(2)N(1)	1.30	1.27
N(1)O(1)O(2)N(2)	-1.21	-1.18
LUMO (eV)	-1.785	-1.847
HOMO (eV)	-5.261	-5.161
ΔE (eV)	3.476	3.314
Dipole moment (D)	3.224	3.844
Chemical Hardness (eV)	1.738	1.657
Molecular length (Å)	42.76	42.76

Table 13: Natural atomic charges and natural electron configuration of selected atoms of the ligands and their complexes with Cu^{2+} evaluated at B3LYP level.

	Atoms	16-opd		16-mpd	
		Charge	Configuration	Charge	Configuration
Ligand	O1	-0.675	[core]$2S^{1.70}2p^{4.96}3d^{0.01}$	-0.670	[core]$2S^{1.70}2p^{4.96}3d^{0.01}$
	O2	-0.675	[core]$2S^{1.70}2p^{4.96}3d^{0.01}$	-0.669	[core]$2S^{1.70}2p^{4.96}3d^{0.01}$
	N1	-0.436	[core]$2S^{1.34}2p^{4.07}3p^{0.01}3d^{0.01}$	-0.436	[core]$2S^{1.34}2p^{4.08}3p^{0.01}3d^{0.01}$
	N2	-0.436	[core]$2S^{1.34}2p^{4.07}3p^{0.01}3d^{0.01}$	-0.434	[core]$2S^{1.32}2p^{4.09}3p^{0.01}3d^{0.01}$
	Atoms	**Cu-16opd**		**Cu-16mpd**	
		Charge	**Configuration**	**Charge**	**Configuration**
Complex	O1	-0.669	[core]$2S^{1.66}2p^{5.00}3p^{0.01}$	-0.671	[core]$2S^{1.67}2p^{4.99}3p^{0.01}$
	O2	-0.669	[core]$2S^{1.66}2p^{5.00}3p^{0.01}$	-0.671	[core]$2S^{1.67}2p^{4.99}3p^{0.01}$
	N1	-0.571	[core]$2S^{1.30}2p^{4.26}3p^{0.01}$	-0.573	[core]$2S^{1.31}2p^{4.25}3p^{0.01}$
	N2	-0.571	[core]$2S^{1.30}2p^{4.26}3p^{0.01}$	-0.573	[core]$2S^{1.31}2p^{4.25}3p^{0.01}$
	Cu	0.964	[core]$4S^{0.34}3d^{9.37}4p^{0.33}$	0.963	[core]$4S^{0.33}3d^{9.38}4p^{0.32}$

4.3 Conclusion:

A new series of nickel(II)-salphen complexes bearing differently substituted aromatic spacer have been successfully synthesised. Low solution electrical conductivity values confirm the non electrolytic nature of the complexes. The ligands are found to be non-mesogenic and non-luminescent, however, all the complexes exhibited unprecedented columnar rectangular structure with *c2mm* symmetry and also exhibited intense blue light emission both in solid state and solution. Based on the spectral and DFT study, a distorted square planar geometry around the Ni(II) centre have been conjectured. The mesomorphic behaviour of the complexes as a function of the spacer substituent is collated.

A series of new oxovanadium(IV)-salphen complexes bearing methyl substituted aromatic spacer have been successfully synthesised. A rare columnar phase transformation behaviour between two rectangular phase both belonging to *c2mm* symmetry is observed upon coordination of the $[N_2O_2]$-donor Schiff base ligand with the metal ion. Two half disc shaped molecules with long alkoxy tail organise themselves in the mesophase via VO. . . . VO . . . . dimeric interaction forming a disc-like shape. An alkoxy chain length dependant marginal variation in the mesomorphic transition and isotropisation temperature was noted. Analogous oxovanadium complexes without any substituent in the aromatic spacer group have been previously shown to exhibit lamello columnar mesomorphism. It would be quite interesting to assess vanadyl complexes with a differently substituted 'salphen' type framework and to explore their mesomorphic behaviour. Cyclic voltammetry displayed a quasi-reversible one-electron response for the VO^{2+}/VO^{3+} redox couple. Based on the spectral and density functional calculations study, a square pyramidal five-coordinate geometry around the VO(IV) centre is conjectured. The work demonstrates that coordination to a vanadyl centre not only induces liquid crystallinity in a non-mesomorphic 'salphen' type ligand bearing long alkoxy tail, but that slight modification in the 'salphen' core can also lead to a quite different mesomorphism furnishing a synthetic handle to tune such properties.

A series of copper-salen complexes with different substituent on the spacer group have been successfully synthesised and their mesomorphic behaviour were investigated. The phase transition behaviour of the compounds as a function of the

spacer group substituent and divalent metal ions has been quite rewarding to explore. The ligands are found to be non-mesomorphic, but their complexes were found to exhibit columnar mesomorphism. The mesophase formation has been shown to be strongly dependant on the substituent of the spacer linkage in salphen group. The copper complex with methyl substituted salen group showed rectangular columnar mesophase (Col_r) and without methyl group showed rectangular columnar plastic mesophase (Col_{rp}). A distorted square planar four coordinate geometry for the newly synthesised complex is proposed on the basis of DFT study.

References:

1. Christopher, J.; Whiteoak, A.; Salassaa, G.; Kleij, A.W. *Chem. Soc. Rev.* **2012,** *41***,** 622.
2. Rezvani, Z.; Ghanea, M.A.; Nejati, K.S.; Baghaei, A. *Polyhedron* **2009**, *28*, 2913.
3. Pucci, D.; Aiello, I.; Bellusci, A.; Callipari, G.; Crispini, A.; Ghedini, M. *Mol. Cryst. Liq. Cryst*. **2009**, *500*, 144.
4. Abe, Y.; Nakabayashi, K.; Matsukawa, N.; Iida, M.; Tanase, T.; Sugibayashia, M.; Ohta, K. *Inorg. Chem. Commun.* **2004**, *7*, 580.
5. Abe, Y.; Nakabayashi, K.; Matsukawa, N.; Takashima, H.; Iida, M.; Tanase, T.; Sugibayashi, M.; Mukai, H.; Ohta, K. *Inorg. Chim. Acta.* **2006**, *359*, 3934.
6. Abe, Y.; Nakazima, N.; Tanase, T.; Katano, S.; Mukai, H.; Ohta, K. *Mol. Cryst. Liq Cryst.* **2007**, *466*, 129.
7. Pucci, D.; Aiello, I.; Bellusci, A.; Crispini, A.; Ghedini, M.; La-Deda, M. *Eur. J. Inorg. Chem.* **2009**, 4274.
8. Cozzi, P.G.; Dolci, L.S.; Garelli, A.; Montalti, M.; Prodi, L.; Zaccheroni, N. *New J. Chem.* **2003**, *27*, 692.
9. Cozzi, P.G. *Chem. Soc. Rev.* **2004**, *33*, 410.
10. Gennari, C.; Piarulli, U. *Chem. Rev.* **2003**, *103*, 3071.
11. Kureshy, R.I.; Ahmad, I.; Khan, N. H.; Abdi, S. H. R.; Pathak, K. *J. Catal.* **2006**, *238*, 134.
12. Abe, Y.; Iyoda, A.; Seto, K.; Moriguchi, A.; Tanase, T.; Yokoyama, H. *Eur. J. Inorg. Chem.* **2008**, 2148.
13. Glebowska, A.; Przybylski, P.; Winek, M.; Krzyczkowaska, P.; Krowczynski, A.; Szydlowska, Z.; Pociecha, D.; Gorecka, E. *J. Mater. Chem.* **2009,** *19*, 1395.
14. Bhattacharjee, C. R.; Das, G.; Mondal, P.; Prasad, S. K.; Rao, D. S. S. *Eur. J. Inorg. Chem.* **2011**, 1418.
15. Bhattacharjee, C. R.; Das, G.; Mondal, P.; Rao, N. V. S. *Polyhedron* **2010**, *29*, 3089.
16. Bhattacharjee, C. R.; Das, G.; Mondal, P. *Liq. Cryst.* **2011**, *38*, 441.

17. Bhattacharjee, C. R.; Das, G.; Mondal, P.; Prasad, S. K.; Rao, D. S. S. *Inorg. Chem. Commun.* **2011**, *14*, 606.
18. Bhattacharjee, C. R.; Das, G.; Mondal, P.; Prasad, S. K.; Rao, D. S. S. *Liq. Cryst.* **2011**, *38*, 615.
19. Bhattacharjee, C. R.; Das, G.; Mondal, P. *Eur. J. Inorg. Chem.* **2011**, 5390.
20. Molard, Y.; Dorson, F.; Circu, V.; Roisnel, T.; Artzner, F.; Cordier, S. *Angew. Chem., Int. Ed.* **2010**, *49*, 3351.
21. Pecinovsky, C.S.; Hatakeyama, E.S.; Gin, D.L. *Adv. Mater.* **2008,** *20*, 174.
22. Feng, X.; Pisula, W.; Zhi, L.; Takase, M.; Mullen, K. *Angew. Chem., Int. Ed.* **2008**, *47*, 1703.
23. Baena, M. J.; Espinet, P.; Folcia, C. L.; Ortega, J.; Etxebarria, J. *Inorg. Chem.* **2010***, 49*, 8904.
24. Arias, J.; Bardaji, M.; Espinet, P.; Folcia, C. L.; Ortega, J.; Etxebarria, J. *Inorg. Chem.* **2009**, *48*, 6205.
25. Binnemans, K. *J. Mater. Chem.* **2009**, *19,* 448.
26. Zheng, H.; Lai, C.K.; Swager, T.M. *Chem. Mater.* **1994**, *6,* 2252.
27. Ghedini, M.; Pucci, D.; Crispini, A.; Bellusci, A.; La Deda, M.; Aiello, I.; Pugliese, T. *Inorg. Chem. Commun.* **2007,** *10,* 243.
28. Kumar, S. *Chem. Soc. Rev.* **2006,** *35*, 83.
29. O'Neill, M.; Kelly, S. M. *Adv. Mater.* **2003**, *15*, 1135.
30. Sergeyev, S.; Pisula, W.; Geerts, Y. H. *Chem. Soc. Rev.* **2007**, *36*, 1902.
31. Shirota, Y.; Kageyama, H. *Chem. Rev.* **2007**, *107*,953.
32. Van de Craats, A.M.; Stutzmann, N.; Nielsen, M.M.; Watson, M. *Adv. Mater.* **2003**, *15*, 495.
33. Laschat, S.; Baro, A.; Steinke, N.; Giesselmann, F.; Hagele, C.; Scalia, G.; Judele, R.; Kapatsina, E.; Sauer, S.; Schreivogel, A.; Tosoni, M. *Angew. Chem., Int. Ed.* **2007**, *46*, 4832.
34. Cavero, E.; Uriel, S.; Romero, P.; Serrano, J.L.; Giménez, R. *J. Am. Chem. Soc.* **2007**, *129*, 11608.
35. Rezvani, Z.; Abbasi, A.R.; Nejati, K.; Seyedahmadian, M. *Polyhedron* **2005**, *24*, 1461.
36. Nejati, K.; Rezvani, Z. *New J. Chem.* **2003**, *27,* 1665.

37. Rezvani, Z.; Ghanea, M.A.; Nejati, K.; Baghaei, S.A. *Polyhedron* **2009**, *28*, 2913.
38. Xing, Y.H.; Han, J.; Zhou, G.H.; Sun, Z.; Zhang, X. J.; Zhang, B.L.; Zhang, Y.H.; Yuan, H. Q.; Ge, M.F. *J. Coord. Chem.* **2008**, *61*, 715.
39. Lin, J. M.; Chen, W. B.; Lin, X. M.; Lin, A. H.; Ma, C. Y.; Dong, W.; Tian, C. E. *Chem. Commun.* **2011**, *47*, 2402.
40. Chattopadhyay, T.; Mukherjee, M.; Banu, K. S.; Banerjee, A.; Suresh, E.; Zangrando, E.; Das, D. *J. Coord. Chem.* **2009**, *62*, 967.
41. Son, H. J.; Han, W. S.; Chun, J. Y.; Kang, B. K.; Kwon, S. N.; Ko, J.; Han, S.J.; Lee, C.; Klm, S. J.; Kang, S.O. *Inorg. Chem.* **2008**, *47*, 5666.
42. Pucci, D.; Crispini, A.; Ghedini, M.; Sezerb, E.I.; La Deda, M. *Dalton Trans.* **2011**, *40*, 4614.
43. Serrette, A.G.; Lai, C.K.; Swager, T.M. *Chem. Mater.* **1994**, *6*, 2252.
44. Trzaska, S.T.; Swager, T.M. *Chem. Mater.* **1998**, *10*, 438.
45. Lee, C.; Yang, W.; Parr, R.G. *Phys. Rev. B* **1988**, *37*, 785.
46. Delley, B. *J. Chem. Phys.* **1990**, *92*, 508.
47. Delley, B. J. *Chem. Phys.* **2000**, *113*, 7756.
48. Delley, B. *J. Phys. Chem.* **1996**, *100*, 6107.
49. Parr, R.G.; Pearson, R.G. *J. Am. Chem. Soc.* **1983**,*105*, 7512.
50. Koopmans, T.A. Physica **1933**, *1*,104.
51. Zhou, Z.; Parr, R.G. *J. Am. Chem. Soc.* **1990**, *112*, 5720.
52. Aihara, J. I. *J. Phys. Chem. A* **1999**, *103,* 7487.
53. Zhou, Z.; Parr, R.G. *J. Am. Chem. Soc.* **1989**, *111,* 7371.
54. Chohan, Z.H.; Sumrra, S. H.; Youssoufi, M. H.; Hadda, T. B. *J. Coord. Chem.* **2010**, *63*, 3981.
55. Yelamaggad, C. V.; Achalkumar, A. S.; Rao, D.S.S.; Prasad, S. K. *J. Mater. Chem.* **2007**, *17*, 4521.
56. Morale, F.; Date, R.W.; Guillon, D.; Bruce, D.W.; Finn, R. L.; Wilson, C.; Blake, A.J.; Schroder, M.; Donnio, B. *Chem. Eur. J.* **2003**, *9*, 2484.
57. Chakravorty, A.; Basu, S. *Nature* **1959**,*184*, 50.
58. Yelamaggad, C.V.; Achalkumar, A. S.; Rao, D. S. S.; Nobusawa, M.; Akutsu, H.; Yamada, J.; Nakatsuji, S. *J. Mater. Chem*. **2008**, *18*, 3433.

59. Glusen, B.; Heitz, W.; Kettner, A.; Wendroff, J. H. *Liq. Cryst.* **1996**, *20,* 627.
60. Binnemans, K.; Lodewyckx, K.; Cardinaels, T.; Parac-Vogt, T. N.; Bourgogne, C.; Guillon, D.; Donnio, B. *Eur. J. Inorg. Chem.* **2006**, 150.
61. Chico, R.; Dominguez, C.; Donnio, B.; Coco, S.; Espinet, P. *Dalton Trans*. **2011**, *40*, 5977.
62. Frisch, M. J.; Trucks, G. W.; Schlegel, H. B.; Scuseria, G. E.; Robb, M. A.; Cheeseman, J.R.; Scalmani, G.; Barone, V.; Mennucci, B.; Petersson, G.A.; Nakatsuji, H.; Caricato, M.; Li, X.; Hratchian, H. P.; Izmaylov, A. F.; Bloino, J.; Zheng, G.; Sonnenberg, J. L.; Hada, M.; Ehara, M.; Toyota, K.; Fukuda, R.; Hasegawa, J.; Ishida, M.; Nakajima, T.; Honda, Y.; Kitao, O.; Nakai, H.; Vreven, T.; Montgomery, J. A.; Peralta, J. E. Jr.; Ogliaro, F.; Bearpark, M.; Heyd, J. J.; Brothers, E.; Kudin, K. N.; Staroverov, V. N.; Kobayashi, R.; Normand, J.; Raghavachari, K.; Rendell, A.; Burant, J. C.; Iyengar, S. S.; Tomasi, J.; Cossi, M.; Rega, N.; Millam, J. M.; Klene, M.; Knox, J. E.; Cross, J. B.; Bakken, V.; Adamo, C.; Jaramillo, J.; Gomperts, R.; Stratmann, R. E.; Yazyev, O.; Austin, A. J.; Cammi, R.; Pomelli, C.; Ochterski, J. W.; Martin, R. L.; Morokuma, K.; Zakrzewski, V. G.; Voth, G. A.; Salvador, P.; Dannenberg, J. J.; Dapprich, S.; Daniels, A. D.; Farkas, Ö.; Foresman, J. B.; Ortiz, J. V.; Cioslowski, J.; Fox, D. J. *Gaussian 09,* Gaussian, Inc.: Wallingford, CT, **2009**.
63. Fleming, I. Frontier orbitals and organic chemical reactions; Wiley: London, **1976**.